Numerical modeling of ground surface deformation related to thrust and reverse fault earthquakes: A discrete element approach.

kchiama@g.harvard.edu

Kristen Chiama[1]; Andreas Plesch[1]; Robb Moss[2]; John H. Shaw[1]

[1]Harvard University, Department of Earth and Planetary Science; [2]California Polytechnic State University

Abstract

Ground surface ruptures during large earthquakes pose significant hazards to urban environments, critical information and energy transmission infrastructure, transportation systems, as well as other sensitive facilities. We seek to improve our physical understanding of the factors that control the style, distribution, and intensity of ground surface ruptures on thrust and reverse faults. Our study combines insights from the patterns of coseismic ground surface ruptures in historic earthquakes as well as the patterns of fault ruptures in analog sandbox fault models to inform the development of a suite of geomechanical models that use the discrete element method (DEM). We explore how various parameters, such as fault geometry and sediment/soil properties, control ground deformation patterns including scarp dip, width, and patterns of secondary folding and fracturing. The DEM method is well suited to this investigation as it can effectively model the geologic processes of faulting at depth, as well as the granular mechanics of soil and sediment deformation in the shallow subsurface. We discuss a suite of models that illustrate characteristic patterns of ground surface deformation and show how these vary as a function of the accumulation of slip on a fault, the fault dip angle, and sediment/soil properties such as density of grain packing and the cohesion and tensile strength of particle bonds. Our initial results show that localized fault scarps are most prominent in cases with stiff sediments and steeply dipping faults (40º to 60º), whereas broader deformation is more prominent with soft sediments and shallowly dipping faults (less than 30º). Fault scarp widths range from 2.0 m to 20 m with wider deformation zones defined by secondary fractures and backthrusts. Furthermore, we show how our DEM models can be designed to evaluate the impact of additional earthquakes occurring between periods of sediment deposition to represent and help interpret patterns commonly found in paleoseismic trenches. Collectively, these results help guide both deterministic and probabilistic assessment of fault rupture hazards.

Introduction

Active thrust faults pose significant earthquake hazards around the world. Events such as the 1999 Chi-Chi (M 7.6), Taiwan, 2008 Wenchuan (M 7.9), China, and 2016 Kaikoura (M7.8), New Zealand earthquakes demonstrate the complex nature of these ruptures, which often exhibit significant components of coseismic folding, faulting, and distributed fracturing (Boncio et al., 2018; Kelson et al., 2001; Nicol et al., 2018; Philip et al., 1992; Xu et al., 2009).

This deformation poses specific hazards for earthquakes that occur in urban environments, impact critical information and energy transmission infrastructure, and transportation systems (Baize et al., 2019; Chang et al., 2015; Kelson et al., 2001; Petersen et al., 2011).

The displacement magnitude, width, and degree of tilting or warping of the ground surface associated with fault traces have an important impact on the ability of built structures to withstand these earthquakes (Boncio et al., 2018; Kelson et al., 2001; Petersen et al., 2011). Moreover, designing and retrofitting facilities require the ability to forecast specific characteristics of future ground surface deformation related to specific faults – a capability that we generally now lack (Chang et al., 2015; Moss et al., 2018; Moss & Ross, 2011; Petersen et al., 2011).

Figure 1: Images of ground surface deformation associated with coseismic thrust and reverse fault displacements: A) 1999 Chi-Chi (M 7.6), Taiwan earthquake (Kelson et al., 2001); B) 2016 Kaikoura (M7.8), New Zealand earthquake (KiwiRail, 2020).

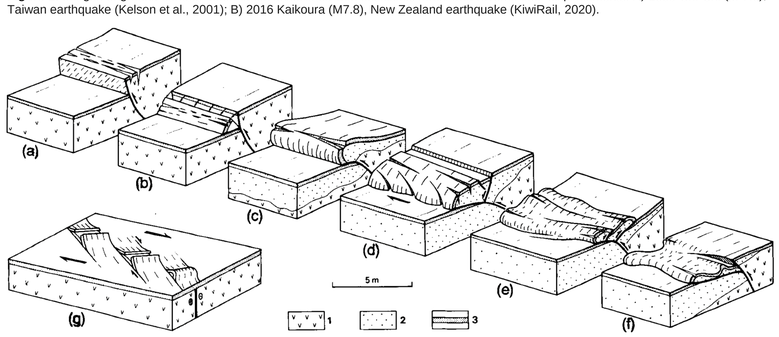

Figure 2: Ground surface deformation along the Spitak fault from the 1988 Armenia (M 6.8) earthquake. The rupture had significant along-strike variations in surface deformation patterns, such as: (A) simple thrust scarp, (B) hanging wall collapse scarp,(C) simple pressure ridge, (D) dextral pressure ridge, (E) backthrust pressure ridge, (F) low angle pressure ridge, and (G) *en echelon* pressure ridge. (Reproduced from Philip et al., 1992; Yeats et al., 1997). (1) bedrock, (2) soft Quaternary sediments, (3) turf.

Data and Methodology

We constructed 2D thrust and reverse fault models using the discrete element method (DEM) to examine the patterns of ground surface deformation related to different sediment and fault parameters. We use Particle Flow Code (PFC2D 7.00), a commercial code based on the initial work of Cundall & Strack (1979) by Itasca (1999).

We ran numerous biaxial stress tests to calibrate the sediment mechanics to natural scales.

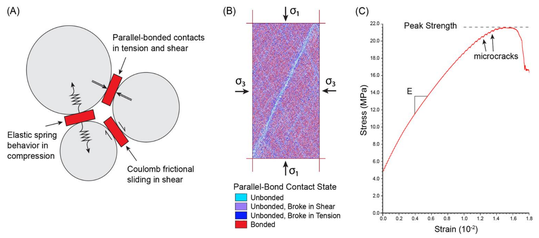

Figure 3: (A) An illustration of DEM inter-particle mechanics for the parallel-bond contact model. (B) A biaxial stress test of numerically modeled material with 2x sand-sized, parallel-bonded particles with a cohesion and tensile strength of 3 MPa. Bonded particles are depicted as red and unbonded particles are blue. (C) The relationship of stress and strain from the biaxial stress test in (B) shows how the peak axial stress at failure and Young's Modulus (E) are obtained with a peak stress of 21.6 MPa and a Young's Modulus of 12.98 with an R^2 of 0.9993.

Further, we replicated analog sandbox fault models such as Cole & Lade (1984).

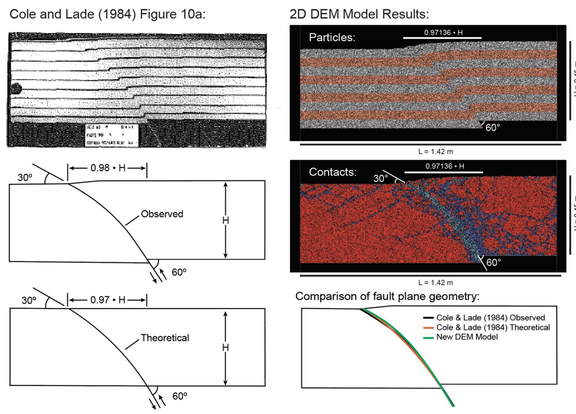

Figure 4: Comparison of the analog Cole & Lade (1984) sandbox fault model (*left*) to a 2D DEM model (*right*) employing the same boundary conditions and sediment parameters with 2x sand-sized, parallel bonded particles. The analog sandbox fault model, observed, and theoretical fault plane geometries presented in Cole & Lade (1984) are reproduced on the left. The sedimentary strata in the DEM model are displayed on the top right for a homogeneous sediment profile and the contact bonds for the same model are shown below. Red contacts are bonded particles while blue are broken contact bonds. The observed and theoretical primary fault planes, as defined by Cole & Lade (1984) for a 60º dipping thrust fault, are remarkably similar to the final 2D DEM result (*bottom right*).

Model Results and Key Parameters

We evaluated a suite of DEM models testing the impact of the the accumulation of slip on a fault, the fault dip angle, and the sediment strength on the resultant ground surface deformation.

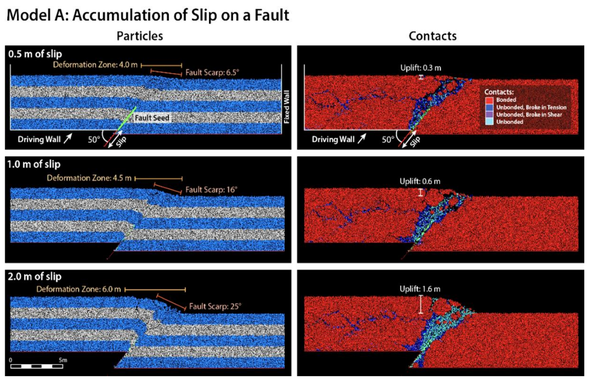

Figure 5: Sequential model showing increase in displacement and the resulting pattern of ground surface deformation. Deformation in the models is driven by displacement of the driving wall parallel to the fault surface. A fault seed is shown in green. *Left*, particles; *right*, particle contacts (blue are broken contact bonds). The top panel shows 0.5 m of slip, the middle panel shows 1.0 m of slip, and the bottom panel shows 2.0 m of slip on a fault that dips 50º. As accumulation of slip on the fault increases, as does the deformation zone width, the fault scarp dip angle, and the amount of uplift observed on the fault scarp.

Figure 6: Comparison of models with different fault dip angles (50º *top*; 20º *bottom*) resulting in different styles of deformation. Left, particles; right, particle bonds (blue are broken bonds). Model A and B feature significant differences in the style of surface deformation. The width of the deformation zone of Model A is limited to the primary fault scarp while the width of the deformation zone in Model B is augmented by backthrusts that form in the hanging wall.

Results

Slip magnitude, fault dip, and sediment strength determine scarp morphology. Extending the terminology of Philip et al. (1992), we recognize 3 distinct classes of fault scarps: simple scarps, hanging wall collapse scarps (low or high cohesion), and direct fault scarp displacements.

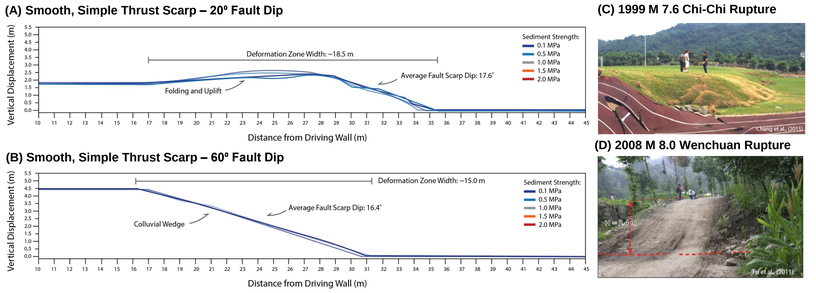

Figure 7: Surface deformation profiles for a set of trials that yield smooth fault scarps for (A) 20º and (B) 60º dipping fault after 5.0 m of accumulated slip. These trials indicate soft sediment strengths (0.1 – 0.5 MPa) yield smooth scarp profiles with a wide zone of deformation and shallow fault scarp dip angles. These surface deformation profiles are similar in morphology to the (C) 1999 Chi-Chi, Taiwan, and (D) 2008 Wenchuan, China ruptures which both had smooth, shallow fault scarps.

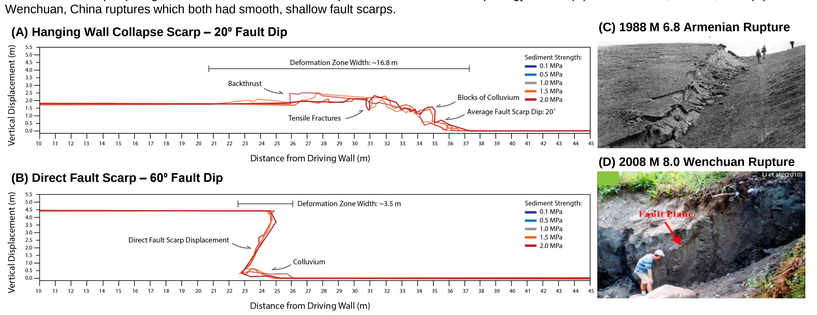

Figure 8: Surface deformation profiles for a set of trials that yield hanging wall collapse scarps and direct fault scarp displacements for (A) 20º and (B) 60º dipping fault after 5.0 m of accumulated slip. These trials indicate stiff sediment strengths (1.5 – 2.0 MPa) yield scarp profiles dominated by brittle fracturing and blocks of colluvium in the toe of the scarp. These trials have smaller zones of deformation compared to the soft sediment trials. Further, these trials feature diverse morphological characteristics such as backthrusts in the 20º fault dip trials and a direct fault scarp displacement in the 60º fault dip trials. These surface deformation profiles are similar in morphology to the (C) 1988 Armenian (hanging wall collapse scarp) and (D) 2008 Wenchuan (direct fault scarp displacement) ruptures.

We can measure the morphological characteristics of the surface deformation profiles to evaluate how the maximum vertical displacement, deformation zone width, and fault scarp dip angle can change with different model parameters such as the accumulation of slip, fault dip angle, and sediment strength.

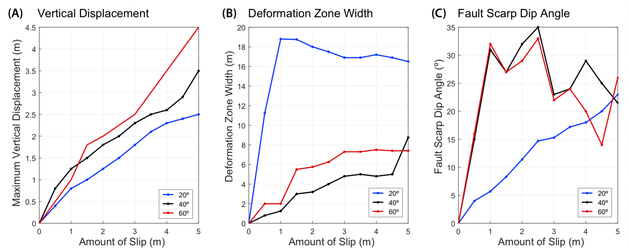

Figure 9: Measurements of the surface deformation characteristics for increasing accumulation of slip on faults dipping 20º (*blue*), 40º (*black*), and 60º (*red*) in moderate strength sediment (1.0 MPa). (A) The maximum vertical displacement of the fault scarp relative to the undeformed surface of the footwall block over increasing accumulations of slip on the fault at depth. (B) The maximum deformation zone width of the fault scarps. (C) Measurements of the average fault scarp dip angle.

Summary & Future Work

Key parameters that influence ground surface deformation:

1. Accumulation of slip on a fault,
   - Increasing slip on a fault at depth yields wider deformation zones, steeper fault scarps, and uplift.
2. Fault dip angle,
   - Steep fault dips localize deformation above the tip of a fault.
   - Shallow faults yield broader zones of deformation including folding, secondary fracturing, and backthrusts.
3. Sediment strength.
   - Soft sediment yields broader, smooth fault scarps with shallow scarp dips.
   - Stiff sediment yields localized brittle deformation or direct fault scarp displacements.

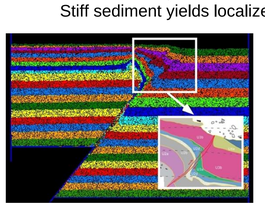

We aim to construct models with alternating sediment deposition and slip on a fault to replicate paleoseismic trenches. The example on the left replicates the trench exposure of the fault that ruptured in the 2008 Wenchuan (M8.0) earthquake (inset from Ran et al., 2019). We aim to model the 1952 Kern County rupture on the White Wolf fault in southern California.

We are inviting fault case studies and ruptures to model in DEM. Please reach out with any suggestions!

Acknowledgements

We would like to thank Benjamin Chauvin for significant contributions to the model framework and guidance throughout this project. We would also like to thank Itasca for coding help and advice while using their software, PFC. Finally, we would like to thank SCEC and NSF for funding and supporting our project.

References

Baize, S., Nurminen, F., Sarmiento, A., Dawson, T., Takao, M., Scotti, O., et al. (2019). A worldwide and unified database of surface ruptures (SURE) for fault displacement hazard analyses. *Seismological Research Letters*, *91*(1), 499–520. https://doi.org/10.1785/0220190144

Boncio, P., Liberi, F., Caldarella, M., & Nurminen, F. C. (2018). Width of surface rupture zone for thrust earthquakes: Implications for earthquake fault zoning. *Natural Hazards and Earth System Sciences*, *18*(1), 241–256. https://doi.org/10.5194/nhess-18-241-2018

Chang, Y. Y., Lee, C. J., Huang, W. C., Hung, W. Y., Huang, W. J., Lin, M. L., & Chen, Y. H. (2015). Evolution of the surface deformation profile and subsurface distortion zone during reverse faulting through overburden sand. *Engineering Geology*, *184*, 52–70. https://doi.org/http://dx.doi.org/10.1016/j.enggeo.2014.10.023

Cole, D. A., & Lade, P. V. (1984). Influence zones in alluvium over dip-slip faults. *Journal of Geotechnical Engineering*, *110*(5), 599–615. https://doi.org/10.1061/(ASCE)0733-9410(1984)110:5(599)

Cundall, P. A., & Strack, O. D. L. (1979). A discrete numerical model for granular assemblies. *Geotechnique*, *29*(1), 47–65.

Fu, B., Shi, P., Guo, H., Okuyama, S., Ninomiya, Y., Wright, S. (2011). Surface Deformation related to the 2008 Wenchuan earthquake, and mountain building of the Longmen Shan, eastern Tibetan Plateau. *Journal of Asian Earth Sciences*, 40(4), 805-824. https://doi.org/10.1016/j.jseaes.2010.11.011.

Itasca. (1999). *PFC2D: Theory and Background. User's Guide, Command Reference, FISH in PFC2D*. Minneapolis, MN, USA: Itasca Consulting Group.

Kelson, K. I., Kang, K. H., Page, W. D., Lee, C. T., & Cluff, L. S. (2001). Representative styles of deformation along the Chelungpu Fault from the 1999 Chi-Chi (Taiwan) earthquake: Geomorphic characteristics and responses of man-made structures. *Bulletin of the Seismological Society of America*, *91*(5), 930–952. https://doi.org/10.1785/0120000741

Moss, R. E. S., & Ross, Z. E. (2011). Probabilistic fault displacement hazard analysis for reverse faults. *Bulletin of the Seismological Society of America*, *101*(4), 1542–1553. https://doi.org/10.1785/0120100248

Moss, R. E. S., Buelna, M., & Stanton, K. V. (2018). Physical, analytical, and numerical modeling of reverse-fault displacement through near-surface soils. *Bulletin of the Seismological Society of America*, *108*(6), 3149–3159. https://doi.org/10.1785/0120180067

Nicol, A., Khajavi, N., Pettinga, J. R., Fenton, C., et al. (2018). Preliminary Geometry, Displacement, and Kinematics of Fault Ruptures in the Epicentral Region of the 2016 *Mw* 7.8 Kaikoura, New Zealand, Earthquake. *Bulletin of the Seismological Society of America*, *108*(3B), 1521–1539. https://doi.org/10.1785/0120170329

Petersen, M. D., Dawson, T. E., Chen, R., Cao, T., Wills, C. J., Schwartz, D. P., & Frankel, A. D. (2011). Fault displacement hazard for strike-slip faults. *Bulletin of the Seismological Society of America*, *101*(2), 805–825. https://doi.org/10.1785/0120100035

Philip, H., Rogozhin, E., Cisternas, A., Bousquet, J. C., Borisov, B., & Karakhanian, A. (1992). The Armenian earthquake of 1988 December 7: faulting and folding, neotectonics and palaeoseismicity. *Geophysical Journal International*, *110*(1), 141–158. https://doi.org/10.1111/j.1365-246X.1992.tb00716.x

Ran, Y., Xu, X., Wang, H., Chen, W., Chen, L., Liang, M., et al. (2019). Evidence of Characteristic Earthquakes on Thrust Faults From Paleo-Rupture Behavior Along the Longmenshan Fault System. *Tectonics*, *38*(7), 2401–2410. https://doi.org/10.1029/2019TC005495

Xu, X., Wen, X., Yu, G., Chen, G., Klinger, Y., Hubbard, J., & Shaw, J. (2009). Coseismic reverse- and oblique-slip surface faulting generated by the 2008 Mw 7.9 Wenchuan earthquake, China. *Geology*, *37*(6), 515–518. https://doi.org/10.1130/G25462A.1

Yeats, R. S. (1997). *The geology of earthquakes*. Oxford University Press.